Progress In Electromagnetics Research M, Vol. 12, 1–15, 2010

A CELL-VERTEX FINITE VOLUME TIME DOMAIN METHOD FOR ELECTROMAGNETIC SCATTERING

N. Deore and A. Chatterjee

Department of Aerospace Engineering
Indian Institute of Technology Bombay
Mumbai 400 076, India

Abstract—A cell-vertex based finite volume scheme is used to solve the time-dependent Maxwell's equations and predict electromagnetic scattering from perfectly conducting bodies. The scheme is based on the cell-vertex finite volume integration method, originally proposed by Ni [1], for solution of the two dimensional unsteady Euler equations of gas dynamics. The resulting solution is second-order accurate in space and time, and requires cell based fluctuations to be appropriately distributed to the state vector stored at cell vertices at each time step. Results are presented for two-dimensional canonical shapes and complex three dimensional geometries. Unlike in gas dynamics, no user defined numerical damping is required in this novel cell-vertex based finite volume integration scheme when applied to the time-domain Maxwell's equations.

1. INTRODUCTION

The Finite Volume Time Domain (FVTD) technique was introduced by Shankar [2] to solve Maxwell's equations in the time domain. Time domain techniques are being increasingly employed to solve the Maxwell's equations due to greater flexibility in dealing with broad-band signals and diverse material properties. FVTD techniques are based on solving time-domain Maxwell's equations in the integral form and allow for a relatively flexible discretization of the solution space. The resulting ability to deal with complex geometries, in the framework of a finite volume discretization, is a major advantage of the FVTD technique over traditional time domain techniques like the Finite Difference Time Domain (FDTD) method [3] based on Cartesian grids. This is of particular interest when dealing with complex configurations

Corresponding author: N. Deore (narendra@aero.iitb.ac.in).

often encountered in simulation of electromagnetic scattering from aerospace configurations. Electromagnetic field variables are also co-located in space and time in the FVTD technique unlike the staggered differencing employed for the FDTD method resulting in an easier implementation. The conservation laws, in integral form, are satisfied at each time step in each control volume in the discretized space in a FVTD framework. Finite volume techniques can also be categorized as cell-vertex or cell-centered based on the relative location of the state vector in the discretized solution space. Cell-vertex finite volume techniques have the state vector located at vertices of control volumes or cells which make up the discretized solution space while the location is at cell centers in case of cell-centered techniques. Cell-vertex techniques allow boundary conditions to be implemented directly on the scatterer surface. This can significantly enhance the ability of a FVTD technique in accurately solving for electromagnetic scattering from complex geometries. Physical conservation laws naturally lead to cell-centered finite volume formulations making them much more common than cell-vertex based finite volume formulations. It is easier to visualize a cell-centered state vector representing cell-averaged quantities which change due to fluxes entering or leaving the control volume. In the present work, a cell-vertex based FVTD method is used to solve for electromagnetic scattering from perfectly conducting geometries in a structured finite-volume discretization. The cell-vertex based finite volume method in this work was originally proposed by Ni [1] to solve the two dimensional (2D), time-dependent, Euler equation of gas dynamics. Ni's cell-vertex based finite volume formulation is a rare instance of a genuinely multidimensional treatment of hyperbolic conservation laws using a cell-vertex based finite volume formulation. The time-domain Maxwell's equations may be expressed as a set of hyperbolic conservation laws when written in total field form which allows for an adaptation of algorithms developed for the time-dependent Euler equations of gas dynamics to the Computational Electromagnetics (CEM) framework [4]. Ni's algorithm can be considered a genuinely multidimensional form of the 'fluctuation-signal' approach proposed by Roe [5] for solving time-dependent wave dominated phenomena. This is different from upwind based cell-vertex schemes which often treat multidimensional problems as a sequence of one-dimensional operations [5]. However, since weights in the distribution formula used in Ni's scheme finally result in a second-order accurate centrally differenced Lax-Wendroff formulation, heavy user-defined damping is essential in strongly nonlinear problems especially shock dominated high-speed flows in gas dynamics [6]. The linear nature of the time-dependent Maxwell equation in free space

may be a more appropriate choice for the application of Ni's novel cell-vertex based finite volume scheme, originally proposed for the non-linear Euler system. An early effort in literature to adapt Ni's [1] novel cell-vertex based finite volume technique to the time-domain Maxwell's equations was restricted to electromagnetic scattering from 2D perfectly conducting geometries with Transverse Magnetic (TM) polarization [7]. In the present work, Ni's cell-vertex based finite volume technique is used to solve for electromagnetic scattering from 2D perfectly conducting geometries with TM and Transverse Electric (TE) polarization and then extended to three dimensional (3D) applications. Extension to 3D is not trivial since the second-order Lax-Wendroff scheme, in the present cell-vertex finite volume formulation, by default, requires a dual cell to approximate the second-order terms which is more complex in 3D. Finite volume discretizations using an O-O topology in 3D can also require special attention to be paid during boundary condition implementation when solved using a cell-vertex formulation.

2. GOVERNING EQUATIONS

Maxwell's curl equations in the differential form for wave propagation in free space can be expressed as

$$\frac{\partial \mathbf{B}}{\partial t} + \nabla \times \mathbf{E} = 0 \tag{1}$$

$$\frac{\partial \mathbf{D}}{\partial t} - \nabla \times \mathbf{H} = 0 \tag{2}$$

where $\mathbf{B}$ is the magnetic induction, $\mathbf{E}$ the electric field vector, $\mathbf{D}$ the electric field displacement, and $\mathbf{H}$ the magnetic field vector. The $\mathbf{B}$ and $\mathbf{D}$ are related to $\mathbf{E}$ and $\mathbf{H}$ through permittivity (ϵ) and the permeability (μ) with $\mathbf{D} = \varepsilon\mathbf{E}$, and $\mathbf{B} = \mu\mathbf{H}$. The above equations can be recast in a conservative total field form as

$$\frac{\partial \mathbf{u}}{\partial t} + \frac{\partial \mathbf{f}(\mathbf{u})}{\partial x} + \frac{\partial \mathbf{g}(\mathbf{u})}{\partial y} + \frac{\partial \mathbf{h}(\mathbf{u})}{\partial z} = 0. \tag{3}$$

where

$$\mathbf{u} = \begin{pmatrix} B_x \\ B_y \\ B_z \\ D_x \\ D_y \\ D_z \end{pmatrix}, \quad \mathbf{f} = \begin{pmatrix} 0 \\ -D_z/\varepsilon \\ D_y/\varepsilon \\ 0 \\ B_z/\mu \\ -B_y/\mu \end{pmatrix}, \quad \mathbf{g} = \begin{pmatrix} D_z/\varepsilon \\ 0 \\ -D_x/\varepsilon \\ -B_z/\mu \\ 0 \\ B_x/\mu \end{pmatrix}, \quad \mathbf{h} = \begin{pmatrix} -D_y/\varepsilon \\ D_x/\varepsilon \\ 0 \\ B_y/\mu \\ -B_x/\mu \\ 0 \end{pmatrix} \tag{4}$$

subscripts indicates scalar components in the Cartesian x, y, z directions. In two dimensions (2D), Maxwell's equations can be split into two sets of systems. These are the equations for Transverse Magnetic (TM) and Transverse Electric (TE) waves. The 2-D conservative form for free space can be expressed as

$$\frac{\partial \mathbf{u}}{\partial t} + \frac{\partial \mathbf{f}(\mathbf{u})}{\partial x} + \frac{\partial \mathbf{g}(\mathbf{u})}{\partial y} = 0. \tag{5}$$

For TM polarization, the vectors $\mathbf{u}$, $\mathbf{f}$, and $\mathbf{g}$ in Equation (5) are

$$\mathbf{u} = \begin{pmatrix} B_x \\ B_y \\ D_z \end{pmatrix}, \qquad \mathbf{f} = \begin{pmatrix} 0 \\ -D_z/\epsilon \\ -B_y/\mu \end{pmatrix}, \qquad \mathbf{g} = \begin{pmatrix} D_z/\epsilon \\ 0 \\ B_x/\mu \end{pmatrix} \tag{6}$$

The corresponding vectors for TE polarization in Equation (5) are,

$$\mathbf{u} = \begin{pmatrix} D_x \\ D_y \\ B_z \end{pmatrix}, \qquad \mathbf{f} = \begin{pmatrix} 0 \\ B_z/\mu \\ D_y/\epsilon \end{pmatrix}, \qquad \mathbf{g} = \begin{pmatrix} -B_z/\mu \\ 0 \\ -D_x/\epsilon \end{pmatrix} \tag{7}$$

3. NUMERICAL TECHNIQUE

Equation (3) can be rewritten in operator form

$$\mathcal{L}(\mathbf{u}) = 0 \tag{8}$$

Decomposing the total field into incident (i) and scattered (s) fields, Equation (8) is written as

$$\mathcal{L}\left(\mathbf{u}^i + \mathbf{u}^s\right) = 0 \tag{9}$$

In the scattered field formulation normally employed for FVTD computations, the incident field is taken to be the solution of the Maxwell's equations in free space and the equations to be solved are [8]

$$\mathcal{L}\left(\mathbf{u}^s\right) = 0. \tag{10}$$

3.1. Finite Volume Discretization

The system of Equation (3) in the conservative form in free space can thus be written in a scattered field formulation as

$$\frac{\partial \mathbf{u}^s}{\partial t} + \frac{\partial \mathbf{f}(\mathbf{u}^s)}{\partial x} + \frac{\partial \mathbf{g}(\mathbf{u}^s)}{\partial y} + \frac{\partial \mathbf{h}(\mathbf{u}^s)}{\partial z} = 0. \tag{11}$$

where superscript s indicates scattered field variables. Integrating the differential form of the conservation law represented by Equation (11) over an arbitrary control volume Ω

$$\frac{\partial \int_\Omega \mathbf{u}^s d\mathcal{V}}{\partial t} + \int_\Omega \boldsymbol{\nabla} \cdot (\mathbf{F}(\mathbf{u}^s)) d\mathcal{V} = 0 \tag{12}$$

and applying the divergence theorem, the integral form of the conservation law is obtained as

$$\frac{\partial \int_{\Omega} \mathbf{u}^s d\mathcal{V}}{\partial t} + \oint_{\mathcal{S}} \mathbf{F}(\mathbf{u}^s) \cdot \hat{\mathbf{n}} d\mathcal{S} = 0 \tag{13}$$

and used to formulate the problem in the FVTD framework. For 3D problems, the domain is discretized into hexahedral cells, and the integral form applied to each cell. The equivalent discretization for 2D problems consists of quadrilateral cells. The state vector is defined at cell centers in a cell-centered formulation and at cell vertices in a cell-vertex formulation. The discretized form for the qth cell in the more common cell-centered formulation is [9]

$$\Omega_q \frac{d\tilde{\mathbf{u}}_q^s}{dt} + \sum_{p=1}^{6} [(\mathbf{F}(\mathbf{u}^s) \cdot \hat{\mathbf{n}}\mathcal{S})_p]_q = 0 \tag{14}$$

where $\tilde{\mathbf{u}}_q^s$ indicates the volume average of $\mathbf{u}^s$ over cell q and $[(\mathbf{F}(\mathbf{u}^s) \cdot \hat{\mathbf{n}}\mathcal{S})_p]_q$ the average flux through face p of cell q and $\mathcal{S}$ is the area of the cell face p with an outer unit normal vector $\hat{\mathbf{n}}$. For two-dimensional problems, the domain is discretized into the quadrilateral cells and the integral form is applied to each cell. The equivalent discretized form in two-dimensional formulations for the qth cell is

$$\mathcal{A}_q \frac{d\tilde{\mathbf{u}}_q^s}{dt} + \sum_{p=1}^{4} [(\mathbf{F}(\mathbf{u}^s) \cdot \hat{\mathbf{n}}s)_p]_q = 0 \tag{15}$$

where $\mathcal{A}_q$ is the cell area. Equations (14) and (15) represent a generic system of hyperbolic conservation laws discretized in a finite volume framework and can be solved using a variety of existing numerical schemes meant for such applications. Numerical schemes usually used to solve hyperbolic conservation laws either have the space and time discretization coupled as in the Lax-Wendroff class of schemes or have them treated separately in a method of lines approach [16].

3.2. Ni's Cell Vertex Based Finite Volume Method

A novel cell-vertex based finite volume scheme originally proposed by Ni [1] for the solution of 2D time-dependent Euler equations of gas dynamics and subsequently extended to 3D Euler equations [10, 12], is adapted to solve the time-dependent Maxwell's equations in a finite volume time domain framework in two and three dimensions. The cell-vertex based finite volume scheme can be considered to belong to the "fluctuation-signal" framework proposed by Roe for the solution

of time-dependent Euler equations of gas dynamics [5]. In Ni's finite-volume time integration scheme, the fluctuation is calculated based on state vector stored at cell vertices and distributed to cell vertices after a discrete time-step in a multidimensional sense. This is different from the upwind based redistribution used by Roe in his cell-vertex based fluctuation-signal framework which forces the redistribution to a sequence of one-dimensional operations based on solving a Riemann problem perpendicular to the cell faces. Though Ni originally claimed the redistribution to be based on wave movement, it can be shown that the finite volume integration scheme proposed by Ni can be expressed as a spatially central-differenced Lax-Wendroff scheme [6] which is second-order accurate in space and time. A second-order update for the state vector $\mathbf{u}$ in Equation (5) based on Taylor series approximation is written as

$$\delta\mathbf{u} = \left(\frac{\partial\mathbf{u}}{\partial t}\right)^n \Delta t + \left(\frac{\partial}{\partial t}\left(\frac{\partial\mathbf{u}}{\partial t}\right)\right)^n \frac{\Delta t^2}{2} \tag{16}$$

Replacing the time derivatives with space derivatives from Equation (5),

$$\delta\mathbf{u} = -\left(\frac{\partial\mathbf{f}}{\partial x} + \frac{\partial\mathbf{g}}{\partial y}\right)^n \Delta t - \left[\frac{\partial}{\partial x}\left(\frac{\partial\mathbf{f}}{\partial\mathbf{u}}\frac{\partial\mathbf{u}}{\partial t}\right) + \frac{\partial}{\partial y}\left(\frac{\partial\mathbf{g}}{\partial\mathbf{u}}\frac{\partial\mathbf{u}}{\partial t}\right)\right]^n \frac{\Delta t^2}{2}. \tag{17}$$

Equation (17) is approximated using a cell-vertex based finite volume formulation. Consider a 2-D discretization in Fig. 1, with four cells A, B, C and D and their corresponding vertices where the state vector is defined. The vertices of cell C are marked as 1, 2, 3 and 4. The discrete numerical "change" $\mathbf{\Delta U_c}$ for a arbitrary quadrilateral cell is

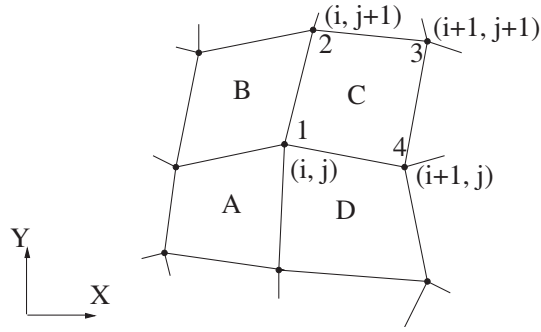

Figure 1. 2-D arbitrary computational cell.

approximated using the divergence theorem as

$$\Delta\mathbf{U_c} = \frac{\Delta t}{\Delta\mathcal{A}}\left(\sum_{p=1}^{4}\left[(\mathbf{F}(\mathbf{u})\cdot\hat{\mathbf{n}}s)_p\right]\right) \tag{18}$$

where $\Delta\mathcal{A}$ is the area of the cell C, s the face length with an outer unit normal vector $\hat{\mathbf{n}}$, Δt is the time step restricted by the Courant-Friedrich-Lewy (CFL) stability criteria. Flux vectors $\mathbf{F}(\mathbf{u})$ are computed for each pth cell face by taking average of the flux vectors stored at vertices of the face. $\Delta\mathbf{U_c}$ is used for the discrete approximation of the first-order term in Equation (16). Unsteady fluxes [1] $\Delta\mathbf{F_c}$ and $\Delta\mathbf{G_c}$, in the Cartesian x and y directions are defined for each cell as

$$\Delta\mathbf{F_c} = \left(\frac{\partial\mathbf{f}}{\partial\mathbf{u}}\right)\Delta\mathbf{U_c}, \qquad \Delta\mathbf{G_c} = \left(\frac{\partial\mathbf{g}}{\partial\mathbf{u}}\right)\Delta\mathbf{U_c} \tag{19}$$

The unsteady fluxes are used to compute second-order contribution in Equation (17) and are based on replacing $(\partial\mathbf{u}/\partial t)$ by $(\Delta\mathbf{U_c}/\Delta t)$. The second-order changes are computed cell-wise by an application of the divergence theorem to cell based unsteady flux values. The components that make up the second-order changes are written as

$$\begin{aligned}\Delta\mathbf{f_c} &= \frac{\Delta t}{\Delta\mathcal{A}}\Big(\Delta\mathbf{F_c}\Delta y^l + \Delta\mathbf{G_c}\Delta x^l\Big)\\ \Delta\mathbf{g_c} &= \frac{\Delta t}{\Delta\mathcal{A}}\Big(\Delta\mathbf{F_c}\Delta y^m + \Delta\mathbf{G_c}\Delta x^m\Big)\end{aligned} \tag{20}$$

where Δx^l, Δy^l, Δx^m and Δy^m (see Fig. 1) are given as [1, 13]

$$\begin{aligned}\Delta x^l &= \frac{1}{2}(x_2 + x_3 - x_1 - x_4)\\ \Delta y^l &= \frac{1}{2}(y_2 + y_3 - y_1 - y_4)\\ \Delta x^m &= \frac{1}{2}(x_3 + x_4 - x_1 - x_2)\\ \Delta y^m &= \frac{1}{2}(y_3 + y_4 - y_1 - y_2)\end{aligned} \tag{21}$$

Implicit in calculation of the above second-order contributions are the definition of pseudo-cell faces of default dual cells for applying the divergence theorem to unsteady cell fluxes. These cell-wise changes are appropriately distributed to cell vertices that make up the cell

as [1],

$$\begin{aligned}(\delta\mathbf{u}_1)_C &= \frac{1}{4}\Big[\Delta\mathbf{U_c} - \Delta\mathbf{f_c} - \Delta\mathbf{g_c}\Big]\\ (\delta\mathbf{u}_2)_C &= \frac{1}{4}\Big[\Delta\mathbf{U_c} - \Delta\mathbf{f_c} + \Delta\mathbf{g_c}\Big]\\ (\delta\mathbf{u}_3)_C &= \frac{1}{4}\Big[\Delta\mathbf{U_c} + \Delta\mathbf{f_c} + \Delta\mathbf{g_c}\Big]\\ (\delta\mathbf{u}_4)_C &= \frac{1}{4}\Big[\Delta\mathbf{U_c} + \Delta\mathbf{f_c} - \Delta\mathbf{g_c}\Big]\end{aligned} \tag{22}$$

It can be shown [5] that these distribution formulas ultimately results in a Lax-Wendroff type distribution. The total correction at grid point 1, $\delta\mathbf{u_1}$, is obtained by adding the contribution from all four neighboring cells sharing vertex 1

$$\delta\mathbf{u_1} = \sum_{m=1}^{4} (\delta\mathbf{u}_1)_m \tag{23}$$

and is added to the state vector at vertex 1 to update to the next time level. The two-dimensional approach can be extended to construct the cell-vertex based finite volume technique in three-dimensions [1]. The first-order numerical change in three-dimension is similarly obtained as

$$\Delta\mathbf{U_c} = \frac{\Delta t}{\Delta\mathcal{V}}\left(\sum_{p=1}^{6}[(\mathbf{F}(\mathbf{u})\cdot\hat{\mathbf{n}}\mathcal{S})_p]\right) \tag{24}$$

where $\Delta\mathcal{V}$ is the volume of cell C. Second-order changes again are a function of cell based unsteady fluxes $\Delta\mathbf{F_c}$, $\Delta\mathbf{G_c}$ and ΔH_c in the Cartesian x, y and z direction. Components of the second-order change are similarly defined as

$$\begin{aligned}\Delta\mathbf{f_c} &= \frac{\Delta t}{\Delta\mathcal{V}}\Big((\Delta\mathbf{F_c} + \Delta\mathbf{G_c} + \Delta\mathbf{H_c})\cdot\mathcal{S}_l\Big)\\ \Delta\mathbf{g_c} &= \frac{\Delta t}{\Delta\mathcal{V}}\Big((\Delta\mathbf{F_c} + \Delta\mathbf{G_c} + \Delta\mathbf{H_c})\cdot\mathcal{S}_m\Big)\\ \Delta\mathbf{h_c} &= \frac{\Delta t}{\Delta\mathcal{V}}\Big((\Delta\mathbf{F_c} + \Delta\mathbf{G_c} + \Delta\mathbf{H_c})\cdot\mathcal{S}_n\Big)\end{aligned} \tag{25}$$

where, $\mathcal{S}_l$, $\mathcal{S}_m$ and $\mathcal{S}_n$ are surface areas and generalization in 3D of face lengths defined in Equation (21) for 2D. Corrections are distributed to the vertices defining cell C using distribution formulas [10],

$$(\delta\mathbf{u}_1)_C = \frac{1}{8}\Big[\Delta\mathbf{U_c} + \alpha_i\Delta\mathbf{f_c} + \alpha_j\Delta\mathbf{g_c} + \alpha_k\Delta\mathbf{h_c}\Big] \tag{26}$$

where, 1 denotes vertex 1 of the cell C, and the parameter $\alpha_{(i,j,k)} = \pm 1$ is based on the relative position of the vertex being updated. In the

interest of brevity, the description in 3D has been kept brief. A detailed description of the 3D treatment for Ni's cell vertex finite volume is available in Refs. [10, 12].

3.3. Boundary Conditions

For perfectly electric conducting (PEC) surfaces, the total tangential electric field $\hat{\mathbf{n}} \times \mathbf{E} = \mathbf{0}$ on the scatterer surface, with $\hat{\mathbf{n}}$ the outward unit normal vector. This condition can be implemented in the scattered field formulation at the perfectly conducting surface as

$$\hat{\mathbf{n}} \times \mathbf{E}^s + \hat{\mathbf{n}} \times \mathbf{E}^i = 0, \tag{27}$$

Since the incident field is known analytically, the tangential component of the scattered electric field on the surface of the scatterer ($\hat{\mathbf{n}} \times \mathbf{E}^s$) can be computed. This boundary condition is directly implemented on the surface of the scatterer in a cell-vertex formulation. Unlike in a cell-centered formulation where "ghost-cells" may be required to be defined for implementing this boundary condition. Standard characteristic boundary conditions can be implemented at the outer boundary with scattered field variables assumed to be negligible at the outer boundary.

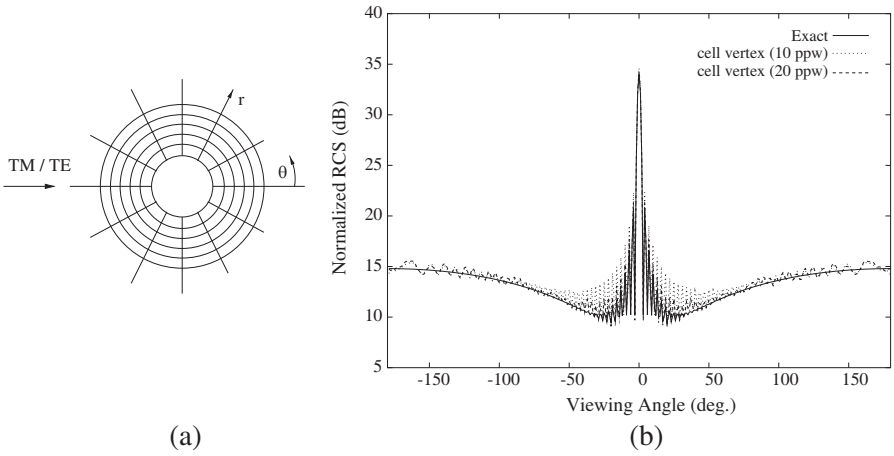

Figure 2. (a) Schematic of grid around circular cylinder. (b) Bistatic RCS, circular cylinder ($a/\lambda = 9.6$, TM).

4. NUMERICAL RESULTS-2D

Ni's cell-vertex finite volume time integration scheme, originally presented for the two-dimensional Euler equations is initially applied to the solution of Maxwells equations in two-dimensions. Results are presented for circular cylinder and NACA 0012 airfoil subject to incident harmonic transverse magnetic (TM) or transverse electric (TE) wave. Both bodies are assumed to be perfectly electric conductors (PEC). Sample bistatic RCS results are presented for a circular cylinder with TM illumination with $a/\lambda = 9.6$, where a is the radius of cylinder and λ the wavelength of the incident harmonic wave. An 'O' topology grid is used with average resolutions of 10 points per wavelength (PPW) and 20 PPW (fine grid). The 'O' grid is shown in schematic form in Fig. 2(a). Results are compared with exact solution and good agreement can be seen in Fig. 2(b). Results are similarly presented for a NACA 0012 airfoil subject to broadside incidence shown in Fig. 3(a). Bistatic RCS for a TE illumination is compared with results in Ref. [11] in Fig. 3(b), and again good agreement is seen. For this test case $a/\lambda = 10$, where a indicates the airfoil chord length.

5. SCATTERING FROM 3D BODIES

The present cell-vertex based FVTD scheme is next extended to compute electromagnetic scattering for three-dimensional geometries. The three-dimensional extension is non-trivial as it can lead to

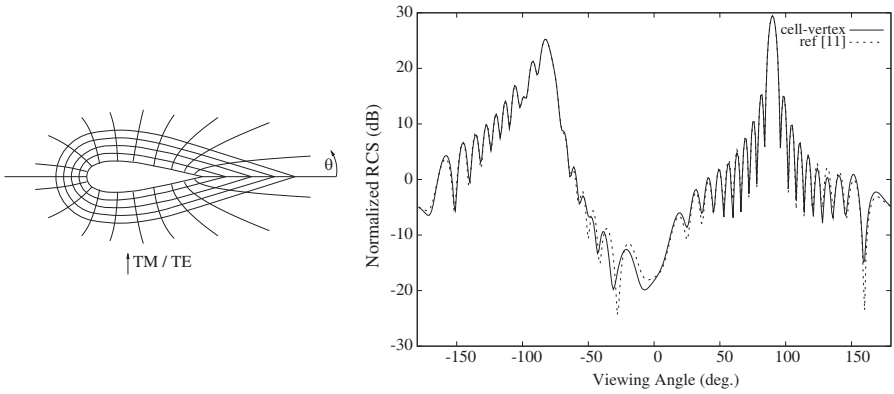

Figure 3. (a) Schematic of grid around NACA 0012 airfoil. (b) Bistatic RCS, NACA 0012 airfoil ($a/\lambda = 10.0$, TE).

complexities not encountered in three-dimensional cell center based finite volume schemes. In principle, cell-vertex based FVTD methods have an advantage over cell-centered schemes as boundary conditions can be directly applied on the scatterer surface. While this is true in general, this might not be always correct for discretizations based on an 'O-O' topology [17], usually used to solve for canonical objects like sphere, almond, etc. O-O topology is normally used to discretize axisymmetric bodies in a single block structured grid framework and is described in detail in Ref. [17]. This discretization results in degenerate points at the two poles. In cell centered finite volume schemes, the degenerate point is not a problem as the conserved variables are stored at cell centers. In a cell vertex method, the values of the state vector at the degenerate point (in an O-O grid) is required to be specified for flux calculations unlike that in a cell centered approach where the degenerate point is redundant. In cell centered finite volume schemes, the face containing the degenerate point has zero area and does not participate in flux calculations (see Fig. 4). In a cell vertex finite volume technique, the degenerate point will also contribute to flux calculations because of cell faces with finite area which also have degenerate points as vertices as shown in Fig. 4 for a sample O-O grid. In the current work, value of the state vectors at a degenerate point, as indicated in Fig. 4 is taken as the average of the state vectors stored at all the neighboring vertices with common index $(k+1)$ in the azimuthal (i) direction.

The present cell-vertex based FVTD scheme is used to solve for electromagnetic scattering from various perfectly conducting 3D

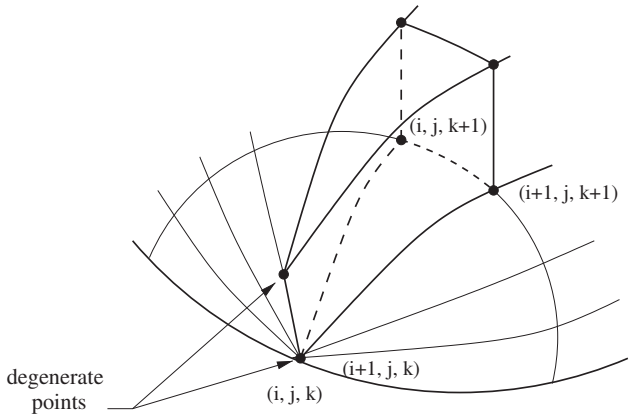

Figure 4. Schematic of a section of O-O grid showing degenerate points.

geometries and compute the RCS. Results are presented for a sphere and NASA almond [14] with discretizations based on O-O topology and a aircraft wing geometry [15] in O-H topology. Fig. 5(a) shows a section of the grid for a PEC sphere discretized using O-O topology. A description of structured grid discretization using O-H topology for aerospace wing geometries is available in Ref. [18]. The monostatic RCS for the sphere is compared with that from exact (Mie series) results around the resonance region in Fig. 5(b). The almond is an

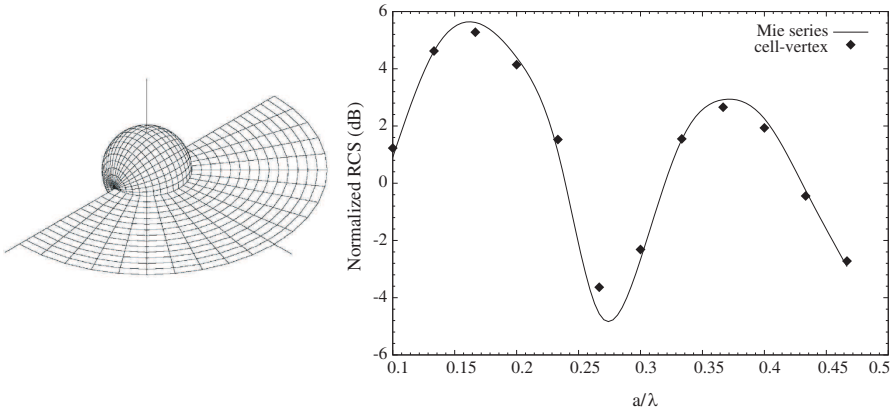

Figure 5. (a) Section of O-O grid, sphere. (b) Monostatic RCS for PEC Sphere.

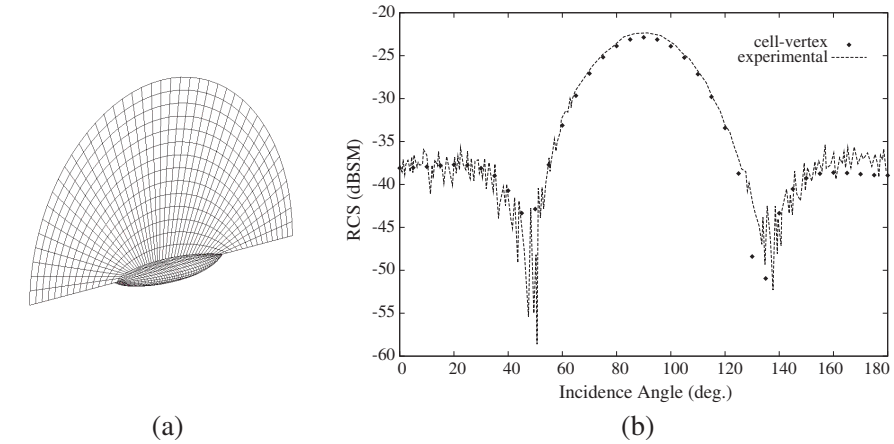

Figure 6. (a) Section of grid around almond. (b) RCS for almond with angle of incidence, 1.19 GHz.

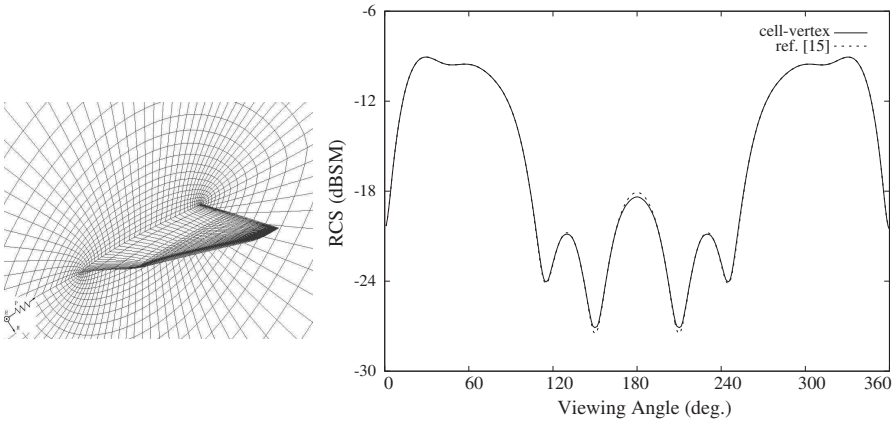

Figure 7. (a) Section of grid around delta wing. (b) Bistatic RCS for delta wing, nose-on incidence ($l/\lambda = 1.4$), H-H polarization.

EMCC benchmark [14], for which experimental results are available. Fig. 6(a) shows a section of the grid around an almond geometry. Fig. 6(b) compares the RCS for different angle of illumination at a frequency of 1.19 GHz (almond length as 9.936 inches). The agreement tends to be good. Similarly Fig. 7(a) shows a delta wing configuration discretized in an O-H topology. Bistatic results at $l/\lambda = 1.4$, where l is the wing span is compared with numerical results in Ref. [15] in Fig. 7(b).

6. CONCLUSION

The FVTD technique because of its inherent capability to model complex geometry and deal with different material properties in a wide range of frequencies is an attractive proposition for simulating electromagnetic scattering for complex geometries and applications. A cell-vertex based finite volume technique based on Ni's novel cell-vertex finite-volume integration method is applied to predict electromagnetic scattering from perfectly conducting bodies. Cell-vertex based finite volume schemes, in principle, can deal with complex geometries more efficiently compared to cell-centered schemes due to a more accurate implementation of boundary conditions on the scatterer geometry. In exceptional case, this might not be true, and approximations are required as shown in the present work for O-O topology based discretizations. Results obtained with the present method in 2D and

3D match well with exact and available results in literature. The current technique was originally proposed for the solution of Euler equations of gas dynamics where heavy numerical damping is required to stabilize the scheme. No such problems are encountered in present applications involving the solution of time-domain Maxwell equations for electromagnetic scattering from perfectly conducting geometries.

REFERENCES

1. Ni, R.-H., "A multiple-grid scheme for solving the Euler equations," *AIAA Journal*, Vol. 20, 1565–1571, 1982.
2. Shankar, V., "A gigaflop performance algorithm for solving Maxwell's equations of electromagnetics," *AIAA Paper*, 91-1578, Jun. 1991.
3. Yee, K., "Numerical solutions of initial boundary value problems involving Maxwell's equations in isotropic media," *IEEE Transactions on Antennas and Propagation*, Vol. 14, 302–307, 1966.
4. Shang, J. S., "Shared knowledge in computational fluid dynamics, electromagnetics, and magneto-aerodynamics," *Progress in Aerospace Sciences*, Vol. 38, No. 6, 449–467, 2002.
5. Roe, P. L., "Fluctuations and signals — A framework for numerical evolution problems," *Numerical Methods in Fluid Dynamics*, K. W. Morton and M. J. Baines (eds.), Academic Press, 219–257, 1982.
6. Hall, M. G., "Cell-vertex multigrid schemes for solution of the Euler equations," *Numerical Methods for Fluid Dynamics II*, K. W. Morton and M. J. Baines (eds.), 303–345, Clarendon Press, Oxford, 1985.
7. Zhu, Y. and J. J. Chattot, "Computation of the scattering of TM plane waves from a perfectly conducting square — Comparisons of Yee's algorithm, Lax-Wendroff method and Ni's scheme," *Antennas and Propagation Society International Symposium*, Vol. 1, 338–341, 1992.
8. Chatterjee, A. and A. Shrimal, "Essentially nonoscillatory finite volume scheme for electromagnetic scattering by thin dielectric coatings," *AIAA Journal*, Vol. 42, No. 2, 361–365, 2004.
9. Chatterjee, A. and R. S. Myong, "Efficient implementation of higher-order finite volume time-domain method for electrically large scatterers," *Progress In Electromagnetics Research B*, Vol. 17, 233–254, 2009.
10. Koeck, C., "Computation of three-dimensional flow using the

Euler equations and a multiple-grid scheme," *International Journal for Numerical Methods in Fluids*, Vol. 5, 483–500, 1985.

11. Shankar, V., W. F. Hall, and A. H. Mohammadin, "A time-domain differential solver for electromagnetic scattering problems," *Proceedings of the IEEE*, Vol. 77, No. 5, 709–721, 1989.
12. Ni, R. H. and J. C. Bogoian, "Prediction of 3-D multistage turbine flow field using a multiple-grid euler solver," *AIAA Paper*, 1–9, 89-0203, Jan. 1989.
13. French, A. D., "Solution of the Euler equations on cartesian grids," *Applied Numerical Mathematics*, Vol. 49, 367–379, 2004.
14. Woo, A. C., H. T. G. Wang, M. J. Schuh, and M. L. Sanders, "Benchmark radar targets for the validation of computational electromagnetics programs," *IEEE Antennas and Propagation Society Magazine*, Vol. 35, No. 1, 84–89, 1993.
15. Chatterjee, A. and S. P. Koruthu, "Characteristic based FVTD scheme for predicting electromagnetic scattering from aerospace configurations," *Journal of the Aeronautical Society of India*, Vol. 52, No. 3, 195–205, 2000.
16. Leveque, R. J., *Finite Volume Methods for Hyperbolic Problems*, Cambridge University Press, Cambridge, UK, 2002.
17. Rossmanith, J. A., "A wave propagation method for hyperbolic systems on the sphere," *Journal of Computational Physics*, Vol. 213, 629–658, 2006.
18. Chakrabartty, S. K., K. Dhanalakshmi, and J. S. Mathur, "Computation of three dimensional transonic flow using a cell vertex finite volume method for the Euler equations," *Acta Mechanica*, Vol. 115, 161–177, 1996.